Extracellular Matrix Stiffness and Architecture Govern Intracellular Rheology in Cancer

Erin L. Baker,[†] Roger T. Bonnecaze,[‡§] and Muhammad H. Zaman[†§*]
[†]Department of Biomedical Engineering, [‡]Department of Chemical Engineering, and [§]Institute of Theoretical Chemistry, The University of Texas at Austin, Austin, Texas

ABSTRACT Little is known about the complex interplay between the extracellular mechanical environment and the mechanical properties that characterize the dynamic intracellular environment. To elucidate this relationship in cancer, we probe the intracellular environment using particle-tracking microrheology. In three-dimensional (3D) matrices, intracellular effective creep compliance of prostate cancer cells is shown to increase with increasing extracellular matrix (ECM) stiffness, whereas modulating ECM stiffness does not significantly affect the intracellular mechanical state when cells are attached to two-dimensional (2D) matrices. Switching from 2D to 3D matrices induces an order-of-magnitude shift in intracellular effective creep compliance and apparent elastic modulus. However, for a given matrix stiffness, partial blocking of β1 integrins mitigates the shift in intracellular mechanical state that is invoked by switching from a 2D to 3D matrix architecture. This finding suggests that the increased cell-matrix engagement inherent to a 3D matrix architecture may contribute to differences observed in viscoelastic properties between cells attached to 2D matrices and cells embedded within 3D matrices. In total, our observations show that ECM stiffness and architecture can strongly influence the intracellular mechanical state of cancer cells.

INTRODUCTION

The mechanical and viscoelastic properties of many biological materials are essential to their underlying function (1). In particular, individual cells have become the focus of several recent investigations aimed at linking their mechanical properties to various physiological and pathological states (2,3). The rheological behavior of individual cells is dictated by the heterogeneous intracellular environment of the cytoplasm (4), the forces exerted on them by the surrounding extracellular matrix (ECM) (5), and the physical attachments that connect the cell interior to the ECM (6). Although numerous inroads have been made in revealing biochemical mechanisms that underlie diseases such as cancer (7), adequate quantitative characterization of associated cellular mechanical properties remains largely incomplete. It is known that cancerous tissue (cancer cells embedded within the ECM) exhibits elevated stiffness compared to normal tissue (8) and that the critical process of cancer cell migration is in part governed by ECM stiffness (9). However, the relationship between the mechanical properties of the ECM and the intracellular mechanical properties that influence cell migration is not well understood.

The construction of the ECM architecture, two-dimensional (2D) versus three-dimensional (3D), imposes an additional factor that is predicted to affect the biophysics of cellular processes, as well as the intracellular mechanical state (9,10). To date, the vast majority of cellular and subcellular mechanical studies have been performed on cells attached to 2D substrates, whereas less attention has been given to the more physiological, realistic 3D matrix environment. Furthermore, nearly all of these cell rheological studies have focused on gels with high stiffness values (on the order of 10^2–10^3 Pa), ignoring softer substrates. Softer substrates may be a better model for cell-matrix interactions within matrices that have been partially degraded by invasive, motile cancer cells. Soft gels have also been employed to examine 3D migration (11), but a clearer understanding of cellular mechanics in these systems remains elusive. Thus, our overall quantitative understanding of intracellular mechanics and interactions with complex and diverse matrices in vivo is quite limited. Given the current state of research, two fundamental questions persist regarding cancer cell mechanics in soft matrix environments: 1), do slight changes in ECM stiffness affect intracellular mechanical properties? and 2), how is this relationship affected by matrix architecture?

In this study, we answer these questions by employing particle-tracking microrheology (PTMR) to investigate the effect of matrix stiffness on the intracellular compliance and stiffness of individual prostate cancer cells both attached to flat 2D matrices and embedded in 3D matrices of identical chemical composition. PTMR is a passive probing method that circumvents many of the sample volume and sample accessibility requirements imposed by extant macrorheological and biophysical techniques (12). PTMR and its advantages have been utilized in recent years to explore the mechanical behavior of several biological organisms and materials (13–15). PTMR has the powerful capability of yielding the time-dependent viscoelastic behavior of a material, as extracted from the thermally driven motions of spherical probes (tracer beads) embedded within passive materials (12). Although particle-tracking rheological protocols have been established (16–19), these techniques have yet to be

Submitted February 10, 2009, and accepted for publication May 29, 2009.

*Correspondence: mhzaman@mail.utexas.edu

Editor: Denis Wirtz.

0006-3495/09/08/1013/9 $2.00

doi: 10.1016/j.bpj.2009.05.054

applied in direct linking of the cytoplasmic mechanical environment of living cancer cells with the mechanics of the surrounding ECM. Here, we examine PC-3 cells with respect to matrices formulated from Type I collagen, which is the major structural protein of the ECM in the human body. We further explore the role of 2D matrix stiffness by utilizing 2D polyacrylamide (PA) gels of variable stiffness and constant pore size and ligand density. Finally, we examine ligand-mediated cell-matrix interactions by partially blocking β1 integrins, which link the cytoskeletal network to the extracellular collagen matrix fibers.

MATERIALS AND METHODS

Cell culture

PTMR experiments were performed on the PC-3 cell line (ATCC, Manassas, VA), which was derived from a metastatic, grade IV tumor originating from the human prostate. Cells were cultured in complete F-12K media (supplemented with 10% fetal bovine serum and 1% penicillin-streptomycin solution (10,000 IU/mL penicillin; 10,000 μg/mL streptomycin)). Cell cultures were maintained in a humidified incubator at 37°C, 5% CO_2. (All cell culture components were purchased from ATCC.)

Collagen matrix preparation and characterization

For 2D matrices, 2.9 mg/mL Type I collagen (BD Biosciences, San Jose, CA) was diluted to three concentrations of 25% (0.73 mg/mL), 37.5% (1.09 mg/mL), and 50% (1.45 mg/mL) v/v with F-12K media; 20 μL of each solution was then evenly spread across the glass-bottom surface (10 mm) of a 35-mm dish (MatTek, Ashland, MA) and exposed to ammonia vapors to promote rapid gelling of the collagen coating across the dish surface. For 3D matrices, 2.9 mg/mL Type I collagen was diluted to concentrations of 25, 37.5, and 50% v/v with cells suspended in complete F-12K media. Each solution (100 μL) was then deposited onto the glass-bottom surface of a 35-mm dish and allowed to gel for 6 h at 37°C, 5% CO_2.

We quantify the matrix stiffness in terms of the bulk elastic modulus of the collagen gel, G_c'. Measurements of G_c' were performed on collagen solutions after they were permitted to gel for 6 h at 37°C, 5% CO_2. A total of 0.7 mL of each gel was measured with a Physica MCR 300 rheometer (Anton Paar, Ashland, VA) operating in parallel plate mode and stressed at 0.1 μN·m oscillatory torque over a frequency range of 0.1–1 Hz. G_c' was approximately constant over the entire frequency range and was measured to be 0.16, 4.71, and 8.73 Pa at a frequency of 1 Hz for gels of concentration 25, 37.5, and 50% v/v, respectively. For all three collagen matrices, the magnitude of G_c' dominated the magnitude of the matrix viscous modulus.

Although we modulate matrix stiffness by varying collagen concentration, we recognize that concentration also influences matrix pore size and the availability of matrix ligands. To ensure that cells were capable of proper ligand-mediated attachment to the matrices resulting from the stated concentrations, we verified that the average cell diameter in 3D matrices (~18–20 μm) was sufficiently larger than the average matrix pore diameters (5.4–13.8 μm) (see Fig. 4 *A*, *inset*). Matrix pore size was measured using ImageJ analysis software (http://rsbweb.nih.gov/ij/) and calculated as the average cross-sectional diameter of pores displayed on scanning electron micrographs (see Fig. S1 *A* in the Supporting Material). A total of five micrographs were obtained from different regions of two samples of each matrix, and a total of 100 pores were measured from each collection of micrographs. We also analyzed the same collection of micrographs to characterize relative ligand density (see Fig. 4 *B*, *inset*). ImageJ was used to binarize the images and then measure the total cross-sectional area of all pores covering each image. The total fiber cross-sectional area was calculated as the reciprocal of the pore area and then normalized by the maximum value obtained across all collagen concentrations. We take this normalized value as a measure of relative ligand density (Fig. S1 *B*).

Polyacrylamide gel preparation and characterization

Two-dimensional PA gels of varying stiffness were prepared as described previously (20). Briefly, a mixture of acrylamide and bis-acrylamide solutions were polymerized with TEMED (Thermo Scientific Pierce, Milford, MA) and 10% ammonium persulfate. Acrylamide concentration was held constant at 3%, with bis-acrylamide concentrations fixed at either 0.04, 0.06, or 0.2%. A total PA solution volume of 20 μL was allowed to polymerize across the glass-bottom surface (30 mm) of a 50-mm dish (MatTek, Ashland, MA). Before depositing the unpolymerized PA solution on the glass-bottom surface, the surface was sequentially pretreated with 0.1 N NaOH, 3-APTMS (Sigma, St. Louis, MO), and 0.5% glutaraldehyde (20). Upon depositing the unpolymerized PA solution on the surface, the solution was flattened using a 22-mm circular glass coverslip (Fisher Scientific, Pittsburgh, PA). Once the polymerization was complete, the coverslip was carefully removed and the surface of the 2D PA gel was cros-slinked with 25% v/v (0.73 mg/mL) Type I collagen. This method yields PA gels of stiffness 50, 200, and 400 Pa (20) (with respect to the bis-acrylamide concentrations noted above) and constant collagen ligand density across the surface (21).

β1 integrin blocking

Blocking of β1 integrins in a 3D collagen matrix of stiffness 4.71 Pa was achieved by supplementing the collagen matrix solution (prepared as described above) with 4b4 antibody (Beckman Coulter, Fullerton, CA) to a final concentration of 10 μg/mL; ~95% of the available β1 integrin receptors are blocked at this antibody concentration (9).

Particle delivery and particle-tracking

PC-3 cells were cultured to ~90% confluency in a 10-cm dish (BD Biosciences) and then embedded with 1.0-μm carboxylated, fluorescent polystyrene tracer beads (Molecular Probes, Carlsbad, CA) using a ballistic particle delivery system (Bio-Rad Laboratories, Hercules, CA) (22). Next, cells were detached using 0.25% Trypsin/0.53 mM EDTA (ATCC). For experiments with 2D matrices, 40 μl of suspended cells were added on top of each previously gelled 2D collagen or PA matrix, as well as on top of an uncoated dish. Each dish was then supplemented with an additional 1.5 mL of media and subsequently incubated for 6 h at 37°C, 5% CO_2. The 6-h incubation period permitted sufficient cell attachment to the matrices without allowing significant cell invasion of the matrices. For experiments with 3D matrices, suspended cells were mixed with Type I collagen and incubated for 6 h at 37°C, 5% CO_2 (see Collagen matrices above). Although the cells may exert physical stresses and send chemical signals (via matrix metalloproteinases, etc.) that locally remodel the matrix to accommodate cell division and cell migration, studies show that the onset of these events typically takes longer to occur than the 6-h incubation period employed here (9), and that these events occur at timescales much longer than that of PTMR analyses (23). Dividing cells were excluded from the PTMR analyses.

After incubation, the 2D (*xy* plane) Brownian motions of individual tracer beads were tracked by imaging each cell culture at 63× for a period of 10 s at a frame rate of 10 Hz using the Leica SP2 AOBS confocal microscope (Leica Microsystems, Bannockburn, IL). A total of 12–18 tracer beads were imaged in each culture. The microscope objective was maintained at 37°C with an objective heater (Bioptechs, Butler, PA). Imaris image analysis software (Bitplane, St. Paul, MN) was then utilized to create particle trajectories in the *xy* plane for each tracer bead. For 2D matrices, the entire experiment was repeated, yielding an average particle count of $N = 33$ and an average cell count of $M = 22$ per collagen matrix formulation and $N = 26$ and $M = 19$ per PA matrix formulation. For 3D matrices without integrin blocking, the entire experiment was repeated twice, yielding $N = 33$ and $M = 20$

per collagen matrix formulation. The particle-tracking experiment was further performed on cells in a 3D matrix of stiffness 4.71 Pa, where $\beta 1$ integrins were partially blocked; the experiment was repeated, yielding $N = 26$ and $M = 22$. Tracer beads used in the analyses were located ≥ 10 μm away from the nearest adjacent bead to avoid effects due to interparticle forces.

Intracellular rheology

Upon tracking the Brownian motions of individual tracer beads, we computed their ensemble-averaged, time-dependent mean-squared displacement (MSD):

$$\left\langle \Delta r^2(\tau)_{xy} \right\rangle = \left\langle [x(t+\tau)-x(t)]^2 \right\rangle + \left\langle [y(t+\tau)-y(t)]^2 \right\rangle, \quad (1)$$

where $\langle \Delta r^2(\tau)_{xy} \rangle$ is the 2D MSD, t is the elapsed time, and τ is the time lag. Since the ensemble-averaged one-dimensional MSD $\langle \Delta x^2(\tau) \rangle$ was found to be approximately equal to $\langle \Delta y^2(\tau) \rangle$ (data not shown), then the total (3D) MSD $\langle \Delta r^2(\tau) \rangle$ was assumed to be isotropic and $\langle \Delta r^2(\tau) \rangle = \langle \Delta x^2(\tau) \rangle + \langle \Delta y^2(\tau) \rangle + \langle \Delta z^2(\tau) \rangle = \frac{3}{2}\langle \Delta r^2(\tau)_{xy} \rangle$. The total ensemble-averaged MSD $\langle \Delta r^2(\tau) \rangle$ was then calculated over N and fit to a two-term power law of the form $\langle \Delta r^2(\tau) \rangle = \beta_1 \tau^{\alpha_1} + \beta_2 \tau^{\alpha_2}$ ($0.95 < R^2 < 0.99$) using a built-in Matlab (The Mathworks, Natick, MA) least-squares algorithm to smooth out trajectory noise.

Given that cells have been established as complex materials that exhibit both elastic and viscous behavior (4), the MSD at any time locally follows a power-law relationship (24), $< r^2(\tau) \sim \tau^{\alpha}$, where α is the diffusive exponent. For a passive material, the diffusive exponent may range from $\alpha = 0$ for a purely elastic solid to $\alpha = 1$ (simple diffusion) for a purely viscous liquid. Between these two viscoelastic extremes, embedded particle motion is described as subdiffusive ($0 < \alpha < 1$) and reflects the relative contribution of a material's elastic and viscous components. However, since living cells are active materials, α reflects not only thermal energy ($k_B T$), but also potential modes of active transport, which cannot be decoupled from thermal energy by particle-tracking measurements (3,16). For such a case, particles may exhibit superdiffusive motion ($\alpha > 1$), and furthermore, $\alpha < 1$ is not a direct, absolute reflection of intracellular viscoelasticity. It has been shown previously that the time-dependent creep compliance of a passive material can be extracted directly from the MSD (25). Since here we examine living, active cells, we describe the intracellular mechanical state in terms of an effective creep compliance J_e (19) and an apparent elastic modulus G'_p, defined by the relationships

$$J_e(\tau) = \frac{\pi a}{k_B T}\left\langle \Delta r^2(\tau) \right\rangle \quad (2)$$

$$G'_p = \left[J_e\big|_{\tau = 1s} \right]^{-1}, \quad (3)$$

where a is the bead radius. Since G'_p is defined at $\tau = 1$ s and not computed from a plateau compliance, we utilize it to describe relative intracellular stiffness as opposed to an absolute measure of intracellular elasticity.

Actin visualization

PC-3 cells were stained with Cellular Lights Actin-GFP (Molecular Probes, Eugene, OR) and then placed atop 2D matrices or embedded within 3D matrices (prepared as described above). Cells were then incubated for 6 h at 37°C, 5% CO_2 and imaged with the LSM 5 Pascal confocal microscope (Carl Zeiss, Thornwood, NY).

RESULTS

Effect of two-dimensional matrix stiffness

PTMR analyses showed that modulation of G'_c with respect to the 2D matrix environment did not significantly alter the Brownian dynamics of embedded tracer beads (Fig. 1 *A*). By extension, neither the intracellular compliance (Fig. 1 *B*) nor the intracellular stiffness was significantly affected as a function of matrix stiffness, with respect to the 2D matrix architecture. Actin micrographs further demonstrate that the architecture of the actin cytoskeletal network is unchanged as 2D matrix stiffness is varied from 0.16 to 8.73 Pa (see Fig. 2 *A*). The effect of 2D matrix stiffness was further explored by holding matrix pore size and ligand density constant. Here, cells were attached to 2D PA gels that were fabricated with varying cross-linker concentrations, which yielded gels of equivalent pore size but differing matrix stiffness (50–400 Pa) (20). The surfaces of all PA gels were then reacted with a fixed concentration of Type I collagen, allowing an equivalent density of cell-matrix ligand binding. Results were similar to those obtained using 2D collagen matrices, and no clear relationship emerges between 2D matrix stiffness and intracellular rheology (Fig. 1 *C*, *inset*). This result suggests that the intracellular mechanical environment of PC-3 cells attached to a 2D matrix may be dominated by biochemical signals, which were not investigated in this experiment. In fact, previous studies have also shown that cell adhesion strength may be insensitive to 2D matrix stiffness for particular cell types (8).

Other studies have reported a positive correlation between 2D matrix stiffness and cell stiffness (26), as well as between 2D matrix stiffness and cell traction forces (8). However, these studies were performed on nontransformed cells, which have been shown to exhibit different substrate-dependent growth (27), cell motility patterns (28), and mechanical features (5,29) compared to transformed cells; furthermore, overall cell stiffness was probed using atomic force microscopy, which measures the combined responses of both internal and cell membrane effects (3), whereas we employed PTMR to measure relative intracellular elasticity. Finally, though cell traction force and internal cell stiffness are related, the former is not a direct predictor of the latter, owing to stress dissipation from the point of cell-matrix attachment through the cell membrane and along the cytoskeletal network (30,31). Thus, our studies provide an additional perspective on cell-matrix interactions, particularly with respect to cancer cells.

When compared to an uncoated glass-bottom surface, the collagen coat induced a significant reduction in the magnitude of the Brownian motion of tracer beads. This result shows that the presence of collagen serves to reduce the effective creep compliance (Fig. 1 *B*), at the same time inversely increasing the apparent elastic modulus of the intracellular environment (not shown). This observation may seem contradictory to previously published studies that reported an increase in cellular stiffness when cells were attached to glass versus a collagen substrate (26). However, not only are the probe, cell type, and substrate chemical identity different in the study reported here, but the stiffness of the underlying substrates used here are orders of magnitude lower than those reported previously. The notable difference

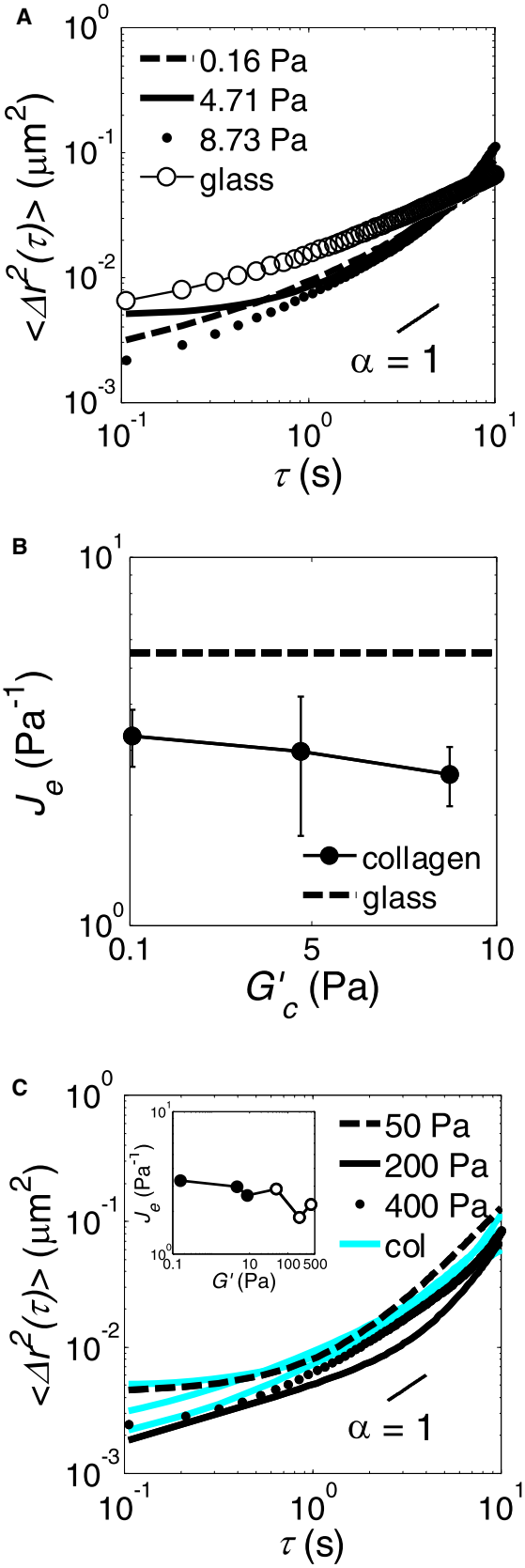

FIGURE 1 Two-dimensional matrix stiffness has little effect on intracellular rheology. (*A*) MSD of 1-μm tracer beads embedded within PC-3 cells that are attached to 2D collagen matrices and cell culture glass (*open-circle line*). Adjusting the matrix stiffness (0.16 (*dashed line*), 4.71 (*solid line*), or 8.73 (*dotted line*) Pa) had little effect on the Brownian dynamics of tracer beads, whereas an uncoated glass-bottom dish induced a higher MSD over most times ($\tau \leq 7$ s). Error bars are omitted for clarity. (*B*) Two-dimensional matrix stiffness has little effect on intracellular effective creep compliance J_e. However, the presence of a collagen matrix induces a less compliant intracellular environment relative to that induced by uncoated glass (*dashed line*). All values of J_e are reported at a time of $\tau = 1$ s. Error bars represent mean $\pm$ SE. (*C*) MSD of 1-μm tracer beads embedded within PC-3 cells that are attached to 2D PA gels. No clear relationship emerges between 2D substrate stiffness (50 (*dashed line*), 200 (*solid line*), or 400 (*dotted line*) Pa) and intracellular rheology. The MSD of cells attached to 2D collagen matrices of stiffness 0.16–8.73 Pa shown for reference (*cyan lines*). (*Inset*) J_e versus 2D substrate stiffness, G', for collagen matrices (*solid circles*) and PA gels (*open circles*). Error bars are omitted for clarity.

in the intracellular mechanical state invoked by glass (which is considered to be infinitely stiff relative to biological gels) (32) highlights the importance of examining cellular responses with respect to physiological substrates as opposed to cells cultured on glass or tissue culture plastic, which may induce mechanical properties that are significantly different from those exhibited in physiological regimes.

Effect of three-dimensional matrix stiffness

In contrast to the 2D system, where small changes in matrix stiffness did not lead to notable changes in intracellular stiffness, modulation of G'_c with respect to the 3D matrix environment had a marked effect on the intracellular mechanical state. First, the magnitude of the ensemble-averaged MSD increased ~5-fold as G'_c increased by nearly a full order of magnitude (from 0.16 to 8.73 Pa) (see Fig. 3 *A*).

Given that matrix stiffness is not independent of matrix pore size and ligand availability, average matrix pore diameters were measured and found to decrease with increasing matrix stiffness (and, by extension, with increasing matrix concentration) (Fig. 4 *A*, *inset*). Relative ligand density was also quantified and found to increase with increasing matrix stiffness (Fig. 4 *B*, *inset*). Since previous studies have also shown that matrix pore size is strongly correlated with matrix concentration and that modulating concentration has a much greater affect on matrix mechanics than it does on ligand-mediated cell-matrix attachment (9,20,33), here we focus our attention on the effect of matrix stiffness (34). The change in effective intracellular creep compliance as a function of G'_c is shown in Fig. 4 *A* at a shear rate of 1 Hz. (J_e is also shown as a function of both G'_c and matrix pore size in Fig. S2 *A*.) Directly proportional to the MSD, J_e increases as the stiffness of the collagen matrix increases. Inversely, the apparent intracellular elastic modulus decreases along with increasing G'_c (Fig. 4 *B* and Fig. S2 *B*). Furthermore, actin micrographs (see Fig. 2 *B*) show that cell morphology was unchanged as 3D matrix stiffness was increased. Taken together, these results suggest that for 3D environments in the range of elasticity examined here, a stiffer, denser ECM may aid in maintaining cell morphology

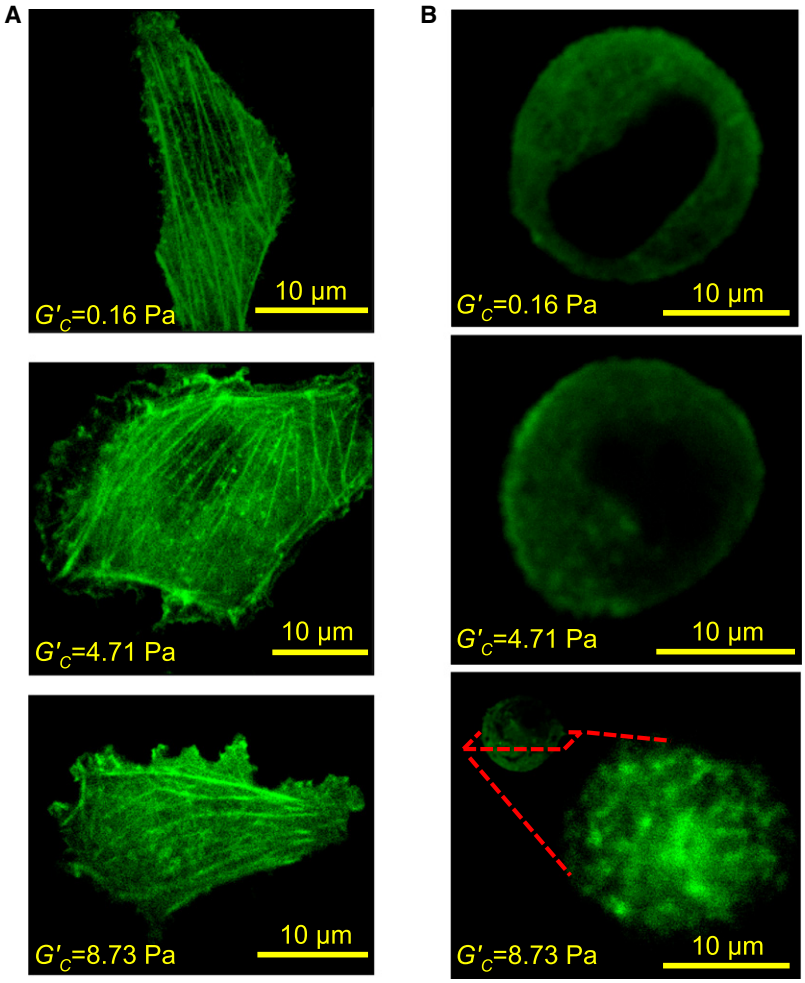

FIGURE 2 Confocal actin micrographs of cells attached to 2D matrices and cells embedded within 3D matrices. (*A*) The actin cytoskeletal architecture of PC-3 cells does not change as the 2D matrix stiffness increases from 0.16 to 8.73 Pa. (*B*) Actin architecture of PC-3 cells embedded within 3D matrices is fundamentally different from that of PC-3 cells attached to 2D matrices; actin fibers are less elongated and defined in 3D matrices. Results suggest that the extent of F-actin polymerization or cross-linking may be affected by changes in 3D matrix stiffness.

in a manner that alleviates the cellular requirement of internal stiffness, thereby yielding a more compliant cytoskeletal filament network. Several previous studies (20,23,33,35,36) suggest that cell morphology depends more on matrix stiffness, matrix dimensionality, and cell type than it does on ligand density or matrix pore size. Spherical, amoeboid-like cell morphology has been associated with a range of soft matrix environments (20,23,33) and with relatively few and less defined actin stress fibers (see Fig. 2 *B*) (11) compared to cells associated with matrices of much higher stiffness.

Three-dimensional versus two-dimensional matrix architecture

In addition to the effect of G'_c on intracellular compliance and stiffness, the 3D matrix architecture invoked an

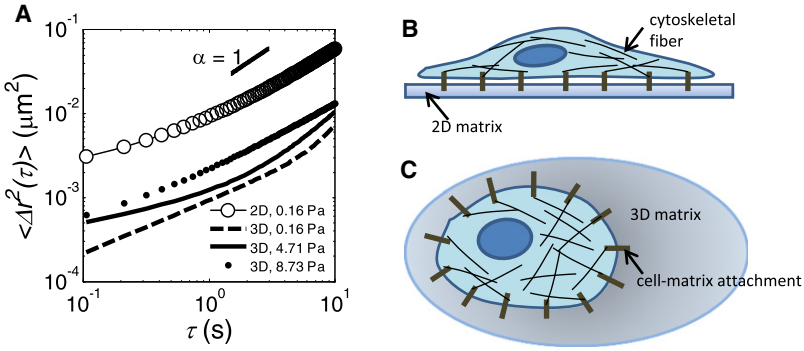

FIGURE 3 MSD of 1-μm tracer beads embedded within PC-3 cells that are attached to a 2D collagen matrix of stiffness 0.16 Pa and embedded within 3D collagen matrices. (*A*) Increasing the 3D matrix stiffness (0.16 (*dashed line*), 4.71 (*solid line*), or 8.73 (*dotted line*) Pa) yielded a clear increase in the magnitude of tracer-bead Brownian dynamics. Compare with MSD for the 2D collagen matrix (*line with open circles*). Switching from a 2D matrix to a 3D matrix architecture induced an order-of-magnitude reduction in the MSD of embedded tracer beads. Error bars are omitted for clarity. (*B*) Schematic of a cell attached to a 2D matrix. (*C*) Schematic of a cell embedded within a 3D matrix. The 2D matrix architecture permits an unengaged free surface over the top (unattached) side of the cell, whereas the 3D matrix architecture engages the cytoskeletal network across the entire cell surface area.

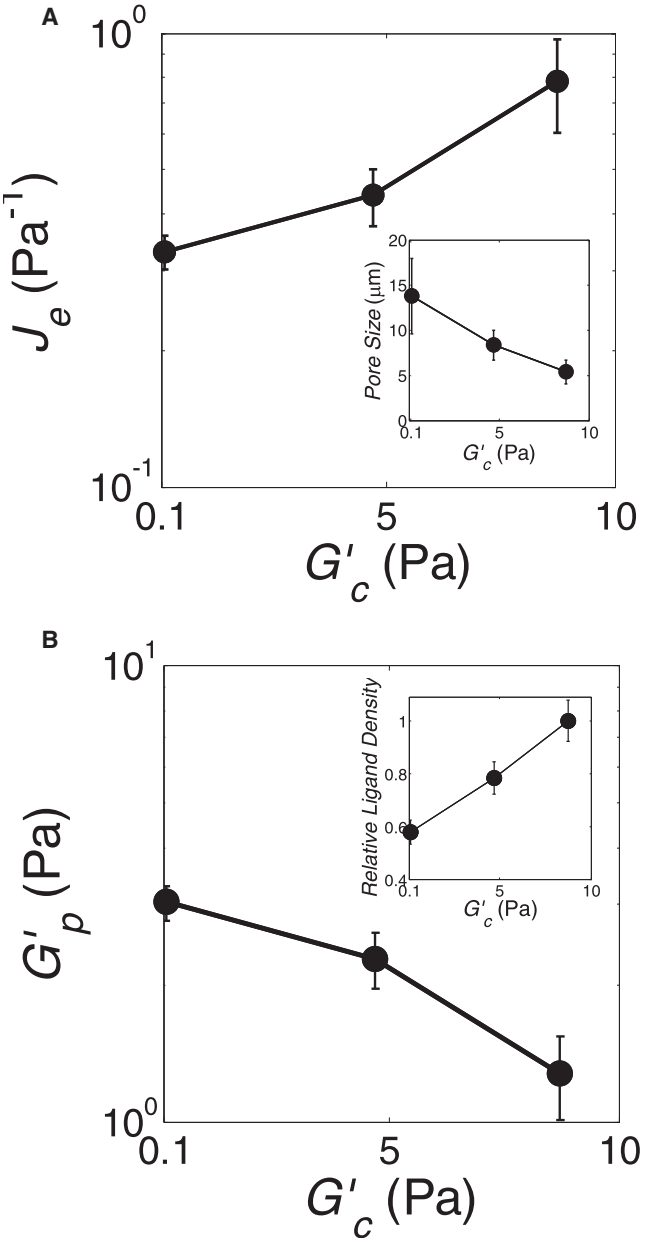

FIGURE 4 Three-dimensional matrix stiffness influences intracellular rheology. (*A*) Intracellular effective creep compliance, J_e, increases as matrix stiffness increases and also as pore size decreases (*inset*). All values of J_e are reported at a time of $\tau = 1$ s. Error bars represent mean ± SE. (*B*) Accordingly, relative intracellular stiffness, G'_p, decreases as matrix stiffness increases and also as ligand density increases (*inset*). Error bars represent mean ± SE.

order-of-magnitude decrease in the MSD of embedded tracer beads relative to the MSD observed with respect to the 2D environment (Fig. 3 *A*). Thus, effective creep compliance observed in 3D (Fig. 4 *A*) is also an order of magnitude lower than that observed in 2D (Fig. 1 *B*), whereas the apparent elastic modulus observed in 3D (Fig. 4 *B*) is an order of magnitude higher than that seen in 2D (not shown). Furthermore, for cells residing within a 3D matrix, partial blocking of β1 integrins (denoted by $3D^{IB}$) yielded an MSD profile of increased magnitude relative to that observed when cells were placed in a 3D matrix of the same stiffness (and pore size) without any integrin blocking (Fig. 5 *A*). Accordingly, the effective creep compliance was increased (Fig. 5 *B*), whereas the apparent elastic modulus was reduced (Fig. 5 *C*), when β1 integrins were blocked. Thus, blocking β1 integrins on cells within a 3D matrix has effectively shifted the intracellular mechanical state toward that of cells attached to a 2D matrix.

DISCUSSION

By utilizing PTMR, we probe how changes in matrix stiffness and matrix architecture of soft gels affect intracellular mechanical properties. Our results suggest that increasing the collagen concentration of a 2D substrate has little influence on intracellular rheology, whereas employing identical compositions in a 3D environment yields a clear relationship between matrix stiffness and intracellular rheology: increasing matrix stiffness was shown to reduce the intracellular apparent elastic modulus and increase the intracellular effective creep compliance. This result may seem contrary to those of previous studies that report increases in cellular stiffness (26), traction forces, and extent of malignant transformation (8) with increased matrix rigidity; however, some important distinctions exist between previous studies and the ones reported here. First, regarding experiments specific to the 3D matrix architecture, previous studies examine integrin clustering and morphology of nonmalignant cell colonies in matrices of varying stiffness (8). However, our studies examine the effect of matrix stiffness on malignant cells in isolation (those attached only to matrix and not to other cells) and do not examine integrin expression as a function of matrix stiffness. Rigidity of normal versus malignant tissues has also been measured using indentation rheometry (8), which yields stiffness of bulk tissue specimens. This is outside the intent of our studies, which do not compare normal cells to cancer cells or measure bulk tissue properties. Rather, our studies employ PTMR to distinguish internal mechanical properties of cancer cells from those of their surrounding matrix; bulk elasticity measurements of tissues do not discriminate contributions from the two components.

Studies performed on 2D substrates have found that integrin clustering and traction forces produced by nonmalignant cells increase with matrix stiffness and that transformed cells exert significantly different magnitudes of traction force compared to their nonmalignant counterpart cells on the same substrates (8,28,29). Other studies have utilized atomic force microscopy and found that 2D substrate stiffness induces cell stiffening (26). However, these experiments do not compare directly to ours. Our results reported here, and several previous studies, have established that cells on 2D matrices can exhibit behaviors drastically different from those of cells within 3D matrices (9,35,37), and this is what we sought to investigate further. In addition, our examination of malignant

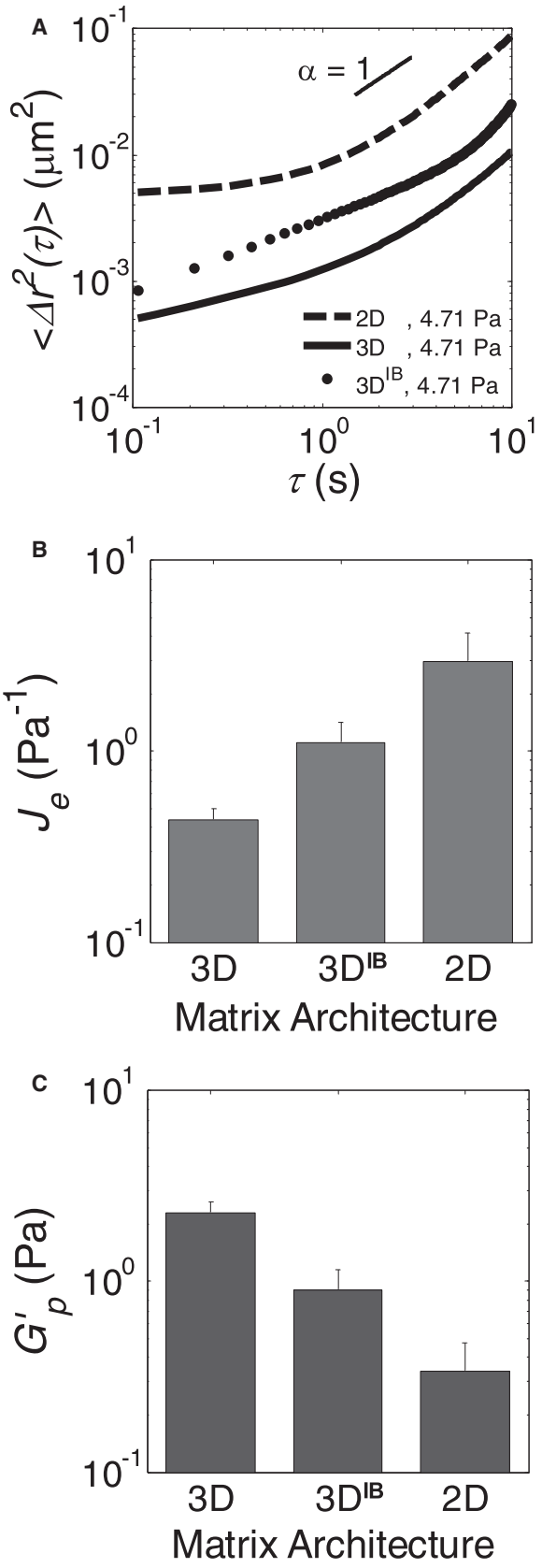

FIGURE 5 Integrin blocking influences intracellular rheology of cells that reside within a 3D matrix. (*A*) MSD of 1-μm tracer beads embedded within PC-3 cells that are attached to a 2D collagen matrix (*dashed line*) and embedded within 3D collagen matrices with β1 integrin blocking ($3D^{IB}$) (*dotted line*) and without integrin blocking (*solid line*). Matrix stiffness is fixed at 4.71 Pa. Addition of 4b4 β1 integrin antibody (10 μg/mL) induces an increase in the magnitude of the MSD relative to cells within a 3D matrix without integrin blocking. Error bars are omitted for clarity. (*B*) For cells embedded within a 3D matrix, effective creep compliance, J_e, increases when β1 integrins are partially blocked. Error bars represent mean ± SE. (*C*) Accordingly, for cells embedded within a 3D matrix, apparent stiffness, G'_p, decreases when β1 integrins are partially blocked. Error bars represent mean ± SE.

cells, which are known to exhibit perturbed mechanical homeostasis (5), offers a different insight into the effect of matrix rigidity on cellular stiffness compared to experiments performed on nonmalignant cells. A decrease in intracellular compliance is indicative of reduced cytoskeletal filament cross-linking (1,34), and/or reduced cytoskeletal filament polymerization (19), yielding shorter filaments or fewer total filaments. This result may have important implications in cancer, where cells migrate through the ECM via a cycle of attachment and forward protrusion after degradation of the ECM (38,39) or, alternatively, via an amoeboid motion whereby cells migrate by flexibly squeezing through pores of the surrounding ECM (40,41). An intracellular softening in response to increased 3D matrix stiffness (and reduced matrix pore size) may confer a motility advantage to cancer cells exhibiting amoeboid migration, which requires cellular deformability and has been associated with diffuse F-actin and diffuse β1 integrin clustering (11). These results may also explain, in part, the differences observed in migration between cells attached to 2D matrices and those embedded within 3D matrices (9), shedding light on the intricate adhesion and signaling mechanisms that affect cell motility (28,29,42). Therefore, our results do not explicitly oppose the findings of previous cellular mechanics studies; in fact, they offer what we believe are new insights into the relationship between extracellular mechanical properties and the intracellular mechanical state in cancer.

In addition to the effect induced within 3D matrices, the 3D matrix environment invokes an order-of-magnitude increase in intracellular stiffness relative to that observed when cells are attached to 2D substrates. We propose that this statistically significant increase in intracellular stiffness results from the increased number of attachments between the cell interior and the extracellular matrix. Increased engagement is inherently invoked by a 3D surrounding, where a cell is connected to the matrix across its entire membrane surface in all directions (Fig. 3 *C*). However, a cell attached to a 2D substrate is only connected across its bottom membrane surface, producing a cell body that is partially engaged, but free across the remainder of its surface (Fig. 3 *B*). In other words, for a given cellular state (e.g., concentration of cell-matrix attachments), a 3D matrix physically presents a higher total number of possible cell-matrix attachments relative to that presented by a 2D substrate, since

the entire cell surface is in contact with a 3D matrix, whereas only part of the cell surface is in contact with a 2D substrate. The free surface imposed by the 2D environment thus permits the cytoskeletal filament network to have a larger degree of freedom, whereas the filament network is more constrained (rigid) when cells reside within a 3D matrix.

It follows that reducing the quantity of cell-matrix attachments should yield a relatively less constrained (more compliant) cytoskeletal filament network for a given matrix architecture. Results shown in Fig. 5, *A–C*, offer convincing evidence of this argument. For cells that reside within a 3D matrix, partial blocking of $\beta 1$ integrins invokes an intracellular mechanical state that is significantly softer (Fig. 5 *B*) than that measured when all integrins remain intact for a matrix of the same stiffness (and pore size). In other words, switching from a 2D to 3D matrix architecture invokes an order-of-magnitude increase in intracellular stiffness; however, when the ligand-mediated interactions that are in part responsible for this increase are partially blocked, the effect of switching to a 3D matrix architecture is mitigated, and cells exhibit a significantly smaller increase in intracellular stiffness relative to that of cells attached to 2D matrices of the same stiffness (Fig. 5 *C*).

Results obtained from integrin blocking have another important implication; for a matrix of given stiffness and pore size, this experiment showed that intracellular compliance increased with decreasing ligand binding (Fig. 5 *B*; compare *3D* with $3D^{IB}$). However, the results obtained without integrin blocking showed that intracellular compliance increased with increasing matrix stiffness (Fig. 4 *A*), and by extension, with increasing ligand availability. Thus, although changing the collagen concentration does affect matrix mechanics and ligand density simultaneously, matrix mechanics appear to exert the dominant influence on the intracellular mechanical environment and override the effect that would otherwise result from varying the ligand availability alone. The reduction in intracellular stiffness measured upon integrin blocking (Fig. 5 *C*; compare *3D* with $3D^{IB}$) is also consistent with previous studies that associate increased integrin expression with increased cell traction forces (8) and with a malignant phenotype (43).

To summarize, our investigations reveal what we believe are novel insights into the effect of ECM stiffness and architecture on the intracellular mechanical state of individual cancer cells. To our knowledge, this study is a first-of-its-kind attempt to probe cellular stiffness in gels that are often used for 3D cell culture and cell migration studies. Cell-matrix interactions observed in these soft gels are distinctly different from those observed in gels with much higher stiffness. Our study provides evidence for two biophysical phenomena that have not been previously described in the context of cell-matrix interactions and cellular rheology. First, we observe that the switch from a 2D to a 3D matrix environment induces an order-of-magnitude shift in the effective intracellular compliance and stiffness, and second, our study demonstrates and quantifies how ECM stiffness regulates effective intracellular compliance and stiffness of cancer cells within a 3D matrix environment. The effect of matrix architecture has important implications for the future of cellular mechanics experiments. It suggests that some cellular systems, such as endothelial cells subjected to a shear flow (44), may be examined in the context of a 2D matrix, whereas others, such as solid tumor cells (5) or endothelial cells within an angiogenic environment (45), may be more appropriately studied within a 3D matrix. Together, these two results improve our fundamental understanding of biophysical phenomena that have important implications in both basic and applied cellular mechanics research.

SUPPORTING MATERIAL

Two figures are available at http://www.biophysj.org/biophysj/supplemental/S0006-3495(09)01115-1.

We thank Dr. David Herrin and his laboratory personnel for providing liberal access to their particle delivery system, as well as Dr. John Wallingford and his lab personnel for providing access to their confocal microscope. We are also grateful to Dr. Denis Wirtz for his valuable advice on the protocol for particle delivery and his comments on an earlier version of this article.

This work was made possible in part by the National Science Foundation-Integrative Graduate Education and Research Trainee (NSF-IGERT) fellowship to E.L.B. M.H.Z. acknowledges the support of the National Institutes of Health (1R01CA132633-01A1).

REFERENCES

1. Levental, I., P. C. Georges, and P. A. Janmey. 2007. Soft biological materials and their impact on cell function. *Soft Matter*. 3:299–306.
2. Suresh, S. 2007. Biomechanics and biophysics of cancer cells. *Acta Biomater*. 3:413–438.
3. Weihs, D., T. G. Mason, and M. A. Teitell. 2006. Bio-microrheology: a frontier in microrheology. *Biophys. J*. 91:4296–4305.
4. Heidemann, S. R., and D. Wirtz. 2004. Towards a regional approach to cell mechanics. *Trends Cell Biol*. 14:160–166.
5. Paszek, M. J., and V. M. Weaver. 2004. The tension mounts: mechanics meets morphogenesis and malignancy. *J. Mammary Gland Biol. Neoplasia*. 9:325–342.
6. Discher, D. E., P. Janmey, and Y. L. Wang. 2005. Tissue cells feel and respond to the stiffness of their substrate. *Science*. 310:1139–1143.
7. Hanahan, D., and R. A. Weinberg. 2000. The hallmarks of cancer. *Cell*. 100:57–70.
8. Paszek, M. J., N. Zahir, K. R. Johnson, J. N. Lakins, G. I. Rozenberg, et al. 2005. Tensional homeostasis and the malignant phenotype. *Cancer Cell*. 8:241–254.
9. Zaman, M. H., L. M. Trapani, A. L. Sieminski, D. Mackellar, H. Gong, et al. 2006. Migration of tumor cells in 3D matrices is governed by matrix stiffness along with cell-matrix adhesion and proteolysis. *Proc. Natl. Acad. Sci. USA*. 103:10889–10894.
10. Panorchan, P., J. S. Lee, T. P. Kole, Y. Tseng, and D. Wirtz. 2006. Microrheology and ROCK signaling of human endothelial cells embedded in a 3D matrix. *Biophys. J*. 91:3499–3507.
11. Wolf, K., I. Mazo, H. Leung, K. Engelke, U. H. von Andrian, et al. 2003. Compensation mechanism in tumor cell migration: mesenchymal-amoeboid transition after blocking of pericellular proteolysis. *J. Cell Biol*. 160:267–277.

12. Mason, T. G., K. Ganesan, J. H. vanZanten, D. Wirtz, and S. C. Kuo. 1997. Particle tracking microrheology of complex fluids. *Phys. Rev. Lett.* 79:3282–3285.

13. Daniels, B. R., B. C. Masi, and D. Wirtz. 2006. Probing single-cell micromechanics in vivo: The microrheology of C-elegans developing embryos. *Biophys. J.* 90:4712–4719.

14. Dawson, M., D. Wirtz, and J. Hanes. 2003. Enhanced viscoelasticity of human cystic fibrotic sputum correlates with increasing microheterogeneity in particle transport. *J. Biol. Chem.* 278:50393–50401.

15. Mason, T. G., T. Gisler, K. Kroy, E. Frey, and D. A. Weitz. 2000. Rheology of F-actin solutions determined from thermally driven tracer motion. *J. Rheol.* 44:917–928.

16. Hoffman, B. D., G. Massiera, K. M. Van Citters, and J. C. Crocker. 2006. The consensus mechanics of cultured mammalian cells. *Proc. Natl. Acad. Sci. USA.* 103:10259–10264.

17. Panorchan, P., J. S. H. Lee, B. R. Daniels, T. P. Kole, Y. Tseng, et al. 2007. Probing cellular mechanical responses to stimuli using ballistic intracellular nanorheology. *Methods Cell Biol.* 83:115–140.

18. Tseng, Y., T. P. Kole, and D. Wirtz. 2002. Micromechanical mapping of live cells by multiple-particle-tracking microrheology. *Biophys. J.* 83:3162–3176.

19. Weihs, D., T. G. Mason, and M. A. Teitell. 2007. Effects of cytoskeletal disruption on transport, structure, and rheology within mammalian cells. *Phys. Fluids.* 19:103102–1.

20. Yeung, T., P. C. Georges, L. A. Flanagan, B. Marg, M. Ortiz, et al. 2005. Effects of substrate stiffness on cell morphology, cytoskeletal structure, and adhesion. *Cell Motil. Cytoskeleton.* 60:24–34.

21. Georges, P. C., W. J. Miller, D. F. Meaney, E. S. Sawyer, and P. A. Janmey. 2006. Matrices with compliance comparable to that of brain tissue select neuronal over glial growth in mixed cortical cultures. *Biophys. J.* 90:3012–3018.

22. Lee, J. S. H., P. Panorchan, C. M. Hale, S. B. Khatau, T. P. Kole, et al. 2006. Ballistic intracellular nanorheology reveals ROCK-hard cytoplasmic stiffening response to fluid flow. *J. Cell Sci.* 119:1760–1768.

23. Dikovsky, D., H. Bianco-Peled, and D. Seliktar. 2008. Defining the role of matrix compliance and proteolysis in three-dimensional cell spreading and remodeling. *Biophys. J.* 94:2914–2925.

24. Gardel, M. L., M. T. Valentine, and D. A. Weitz. 2005. Microrheology. *In* Microscale Diagnostic Techniques. K. Breuer, editor. Springer Verlag, New York.

25. Xu, J. Y., V. Viasnoff, and D. Wirtz. 1998. Compliance of actin filament networks measured by particle-tracking microrheology and diffusing wave spectroscopy. *Rheol. Acta.* 37:387–398.

26. Solon, J., I. Levental, K. Sengupta, P. C. Georges, and P. A. Janmey. 2007. Fibroblast adaptation and stiffness matching to soft elastic substrates. *Biophys. J.* 93:4453–4461.

27. Wang, H. B., M. Dembo, and Y. L. Wang. 2000. Substrate flexibility regulates growth and apoptosis of normal but not transformed cells. *Am. J. Physiol. Cell Physiol.* 279:C1345–C1350.

28. Harris, A. K., D. Stopak, and P. Wild. 1981. Fibroblast traction as a mechanism for collagen morphogenesis. *Nature.* 290:249–251.

29. Munevar, S., Y. L. Wang, and M. Dembo. 2001. Traction force microscopy of migrating normal and H-ras transformed 3T3 fibroblasts. *Biophys. J.* 80:1744–1757.

30. Lauffenburger, D. A., and A. F. Horwitz. 1996. Cell migration: a physically integrated molecular process. *Cell.* 84:359–369.

31. Rosenbluth, M. J., A. Crow, J. W. Shaevitz, and D. A. Fletcher. 2008. Slow stress propagation in adherent cells. *Biophys. J.* 95:6052–6059.

32. Flanagan, L. A., Y. E. Ju, B. Marg, M. Osterfield, and P. A. Janmey. 2002. Neurite branching on deformable substrates. *Neuroreport.* 13:2411–2415.

33. Engler, A., L. Bacakova, C. Newman, A. Hategan, M. Griffin, et al. 2004. Substrate compliance versus ligand density in cell on gel responses. *Biophys. J.* 86:617–628.

34. Lutolf, M. P., and J. A. Hubbell. 2003. Synthesis and physicochemical characterization of end-linked poly(ethylene glycol)-co-peptide hydrogels formed by Michael-type addition. *Biomacromolecules.* 4:713–722.

35. Kenny, P. A., G. Y. Lee, C. A. Myers, R. M. Neve, J. R. Semeiks, et al. 2007. The morphologies of breast cancer cell lines in three-dimensional assays correlate with their profiles of gene expression. *Mol. Oncol.* 1:84–96.

36. Georges, P. C., and P. A. Janmey. 2005. Cell type-specific response to growth on soft materials. *J. Appl. Physiol.* 98:1547–1553.

37. Cukierman, E., R. Pankov, D. R. Stevens, and K. M. Yamada. 2001. Taking cell-matrix adhesions to the third dimension. *Science.* 294:1708–1712.

38. Lo, C. M., H. B. Wang, M. Dembo, and Y. L. Wang. 2000. Cell movement is guided by the rigidity of the substrate. *Biophys. J.* 79:144–152.

39. Raeber, G. P., M. P. Lutolf, and J. A. Hubbell. 2008. Part II: Fibroblasts preferentially migrate in the direction of principal strain. *Biomech. Model. Mechanobiol.* 7:215–225.

40. Brunner, C. A., A. Ehrlicher, B. Kohlstrunk, D. Knebel, J. A. Kas, et al. 2006. Cell migration through small gaps. *Eur. Biophys. J.* 35:713–719.

41. Wolf, K., and P. Friedl. 2006. Molecular mechanisms of cancer cell invasion and plasticity. *Br. J. Dermatol.* 154:11–15.

42. Mofrad, M. R. K. 2009. Rheology of the cytoskeleton. *Annu. Rev. Fluid Mech.* 41:433–453.

43. Weaver, V. M., O. W. Petersen, F. Wang, C. A. Larabell, P. Briand, et al. 1997. Reversion of the malignant phenotype of human breast cells in three-dimensional culture and in vivo by integrin blocking antibodies. *J. Cell Biol.* 137:231–245.

44. Dangaria, J. H., and P. J. Butler. 2007. Macrorheology and adaptive microrheology of endothelial cells subjected to fluid shear stress. *Am. J. Physiol. Cell Physiol.* 293:C1568–C1575.

45. Zhou, X. M., R. G. Rowe, N. Hiraoka, J. P. George, D. Wirtz, et al. 2008. Fibronectin fibrillogenesis regulates three-dimensional neovessel formation. *Genes Dev.* 22:1231–1243.